



Soft Matter

**Elucidating Structure of Donor-acceptor Conjugated
Polymer Aggregates in Liquid Solution**

Journal:	<i>Soft Matter</i>
Manuscript ID	SM-ART-10-2023-001458.R1
Article Type:	Paper
Date Submitted by the Author:	28-Dec-2023
Complete List of Authors:	Saha, Chinmoy; Mississippi State University, Dave C. Swalm School of Chemical Engineering Huda, Masrul; Mississippi State University, Chemical Engineering Sabuj, Md Abdus; Mississippi State University, Dave C. Swalm School of Chemical Engineering and Center for Advanced Vehicular Systems Rai, Neeraj; Mississippi State University, Dave C. Swalm School of Chemical Engineering

SCHOLARONE™
Manuscripts

Cite this: DOI: 00.0000/xxxxxxxxxx

Elucidating Structure of Donor-acceptor Conjugated Polymer Aggregates in Liquid Solution[†]

Chinmoy Saha,^a Md Masrul Huda,^{a‡} Md Abdus Sabuj,^{a‡} and Neeraj Rai^{*a}Received Date
Accepted Date

DOI: 00.0000/xxxxxxxxxx

High-spin donor-acceptor conjugated polymers are extensively studied for their potential applications in magnetic and spintronic devices. Inter-chain charge transfer among these high-spin polymers mainly depends on the nature of the local structure of the thin film and π -stacking between the polymer chains. However, the microscopic structural details of high-spin polymeric materials are rarely studied with an atomistic force field, and the molecular-level local structure in the liquid phase remains ambiguous. Here, we have examined the effects of oligomer chain length, side chain, and processing temperature on the organization of the high-spin cyclopentadithiophene-benzobisthiadiazole donor-acceptor conjugated polymer in chloroform solvent. We have found that the oligomers display a range of ordered aggregation depending on their chain length, with an average π -stacking distance of 3.38 ± 0.03 Å (at $T = 298$ K), showing good agreement with the experiment. Also, the oligomers with longer alkyl side chains show better solvation and shorter π -stacking distance. Furthermore, the clusters grow faster at the higher temperature with more ordered aggregation between the oligomer chains.

1 Introduction

Organic semiconductors (OSCs) with a high-spin (total spin quantum number, $S \geq 1$) ground-state are technologically relevant in the emerging optoelectronic, magnetic, and spintronic applications.^{1–5} Open-shell donor-acceptor conjugated polymers (DACPs) with a high-spin ground-state show distinct optical, electronic, and magnetic properties than their counterpart low-spin closed-shell polymers^{6–10}. The unique optical and magnetic properties of the high-spin polymers make them suitable for potential applications in organic magnetic, spintronic, medical imaging, memory, and charge storage devices. Even though a significant effort is underway in designing and characterizing high-spin conjugated polymers,^{3,7–11} their molecular-level details and dynamics in the liquid solutions are not well understood.

The local structure of a polymer chain aggregates in solution is governed by its molecular weight, side chain positions, bulkiness, and the planarity and curvature of the conjugated backbone.^{12,13}

Polymers of different lengths can adopt different conformations and dynamics that can significantly affect the aggregate formation and local structure.^{14,15} Due to the low solubility of DACPs in solvents, side chains are incorporated to improve the solubility and crystallinity of the polymers. However, the device performance is dependent on the position¹⁶, type,¹⁷ and length¹⁸ of the side chain added to the conjugated backbone of the polymers. Also, a more planar chain backbone ensures a closer π -stacking distance and better charge transfer.¹⁹ Therefore, a deeper understanding of these parameters on the aggregation behavior of high-spin polymers can provide the pathway to control crystallization behavior, even optoelectronic properties.²⁰ Furthermore, the polymer film morphology and photoelectric device performance²¹ are also dependent on the polymer chain conformation and dynamics^{22,23}, solvent and inter-chain interaction,²⁴ and processing conditions (temperature, concentration, density, aging, etc.)^{13,25,26} Such as a more planar backbone and ordered aggregation in the active layer of thin-film improves charge transfer ability.^{27,28} The aggregates formed in the precursor solution significantly impact thin-film structure as the same planar structure and intermolecular stacking arrangement remain preserved in the film following the solution processing and annealing.^{29–31} However, the molecular-level information remains unclear or even unavailable because of the complex interactions³² between the polymer chain and the different factors affecting device performance. Therefore, a better understanding of the local solvation details, such as aggregation, entanglement, and local structural order of large polymeric materials, can shed light on their thin-film mor-

^a Dave C. Swalm School of Chemical Engineering, and Center for Advanced Vehicular System, Mississippi State University, Mississippi State, MS-39762, USA. Fax: +1 662 325 2482; Tel: +1 662 325 0790; E-mail: neerajrai@che.msstate.edu

[†] Electronic Supplementary Information (ESI) available: The supplementary information file contains partial atomic charges in different implicit solvent models, radius of gyration and their correlation lengths, dihedral potential scans and analytic fit, initial system snapshots, and probability distribution of different physical properties. Sample input files are provided on the GitHub: https://github.com/MSELRai/Self_assembly_CPDTBTT. See DOI: 00.0000/00000000.

[‡] These authors contributed equally to this work.

phology and charge transport mechanism.^{33,34}

Polymer chains interact through “weak” non-covalent interactions often classified as the π - π -interaction, van der Waals interactions, or dipole-dipole forces, leading to an aggregation or self-assembly in the solution.^{35,36} Nano- and mesoscale self-assembly of conjugated polymers control the charge transfer through the active layer. The self-assembled polymer chains have a two-dimensional charge transport path.³⁷ The charge transport along the molecular framework occurs through the π -conjugated backbone and the inter-chain charge hopping occurs towards the π -stacking directions as shown in Fig. 1 (A).^{12,38} In addition to the π -conjugation and π -stacking orientation with respect to a substrate surface determines which polymer is suitable for a specific device. For example, the polymer that shows an edge-on orientation, where the aromatic plane remains perpendicular to the substrate surface, and the charge transport occurs parallel to the substrate surface (see Fig. 1B), are better suited for transistor application. On the other hand, polymers with a face-on orientation are better suited for photovoltaic devices.^{12,39,40} Therefore, if we can determine the specific orientation of a particular polymeric material aggregates, we can design optoelectronic devices with optimal performance.

Here, we systematically examined the aggregation behavior of the high-spin cyclopentadithiophene-benzobisthiadiazole (CPDT-BBT) donor-acceptor conjugated polymer (Fig. 2) along with the local chain conformation and dynamic evolution in the chloroform solvent with molecular dynamics (MD) simulation. Chloroform is a common solvent used in the synthesis of conjugated polymers.⁴¹ The CPDT-BBT polymer has a very high open-shell diradical character due to the recovery of aromatic stabilization energy in the thiadiazole units of the BBT acceptor and the thiophene rings of the CPDT donor (demonstrated in our previous work).⁸ A significant open-shell character inherent to the CPDT-BBT polymer localizes the unpaired spins at the two opposite ends of the polymer backbone, reducing electron-electron repulsion and stabilizing a high-spin triplet ground-state at the neutral form.^{8,10} We have investigated the effects of the oligomer chain length (for $n = 2, 4, 8, 16$), linear alkyl side chains (SC4, SC8, SC12, and SC16), branching positions at alkyl side chains (BC2 and BC8), and temperature ($T = 298$ and 323 K) on the aggregation behavior of the CPDT-BBT polymer. The higher temperature speeds up the system dynamics; however, we are somewhat constrained in how high a temperature we can simulate as chloroform, used as the solvent, has 334.5 K as the boiling point.

2 Computational Methodologies

We have utilized the transferable potentials for phase equilibria (TraPPE)^{42–46} force field parameters to capture the non-bond interactions in our model. The bonded parameters, on the other hand, were determined either using density functional theory (DFT) calculations or taken from the optimized potentials for liquid simulations (OPLS)⁴⁷ force field. We opted for the long-range corrected functional, ω B97XD⁴⁸, to address the electron self-interaction error commonly observed in traditional DFT functionals.⁴⁹ These functionals help to mitigate the overdelocalization of electron density, particularly in conjugated molecules, which

tends to overestimate the torsion potential and stabilize the planar conformation with extended π -conjugation.^{50–53} As a result, they have emerged as the preferred choice for accurately modeling complex conjugated systems like DACPs.

The quantum mechanical calculations were performed using the Gaussian16⁵⁴ package. We optimized the geometry of CPDT-BBT and chloroform using the ω B97XD theory and the 6-311G(d,p) basis set. The equilibrium bond lengths and angles were taken from the optimized structure. The angle and dihedral force constants were taken from the OPLS-AA⁴⁷ force field, while a few specific dihedrals were parameterized using DFT calculations. To accomplish this, we performed a dihedral potential surface scan with 10° steps using a monomer fragment, which helped reduce the computational costs. The resulting potential was fitted to the Ryckaert-Bellemans model, as shown in Fig. S1. We have also assessed the impact of considering the whole molecule by comparing the scanned dihedral angles with the ethyl side chain (Fig. S1(C)) or with the acceptor unit (Fig. S1(D)) to the parameters derived from the fragmented structure (Fig. S1(A)). The results demonstrated no significant effect of considering the entire molecule. In our system, the monomers were connected in the trans position, corresponding to the conformation with lower energy. The energy plot in Fig. S2 confirms that the trans configuration (180°) has lower energy compared to the cis configuration (0°). The improper dihedral parameters for our system were generated using the LigParGen.⁵⁵

Due to the diffuse and delocalized nature of charge density in aromatic compounds, the partial charges for the atoms in the aromatic ring are not transferable. Therefore, using the TraPPE force field approach, we calculated the partial atomic charges using the CM5⁵⁶ charge model with 1-octanol as the implicit solvent.⁴⁵ The charge calculations for longer oligomers showed that the partial charges associated with the donor and acceptor moieties at the chain ends remained similar to those of the dimer at the edges. However, the partial atomic charges associated with the core moieties were sensitive to the oligomer size but converged to an asymptotic value at the tetramer stage. Additionally, we performed partial charge calculations using alternative implicit solvents, specifically chlorobenzene and chloroform. The results obtained with these solvents showed no significant differences compared to the 1-octanol solvent model. The maximum observed difference in partial charges was $0.005 |e|$, indicating consistency up to two decimal places, as presented in Table S1.

2.1 Molecular Dynamics Simulation

The initial system, consisting of CPDT-BBT oligomers solvated in chloroform solvent, was generated using the PACKMOL package⁵⁷ (see Fig. S3). In this approach, we randomly placed the CPDT-BBT oligomers and chloroform solvent molecules within the simulation box. The radial distribution of the aromatic ring centers within the oligomers is presented in Fig. S3(B), demonstrating that the oligomers are distributed randomly, without any evident pre-stacking arrangement (as visualized in Fig. S3(C) and S3(D)). This absence of pre-stacking organization is further supported by the density distribution, depicted as a heat map, show-

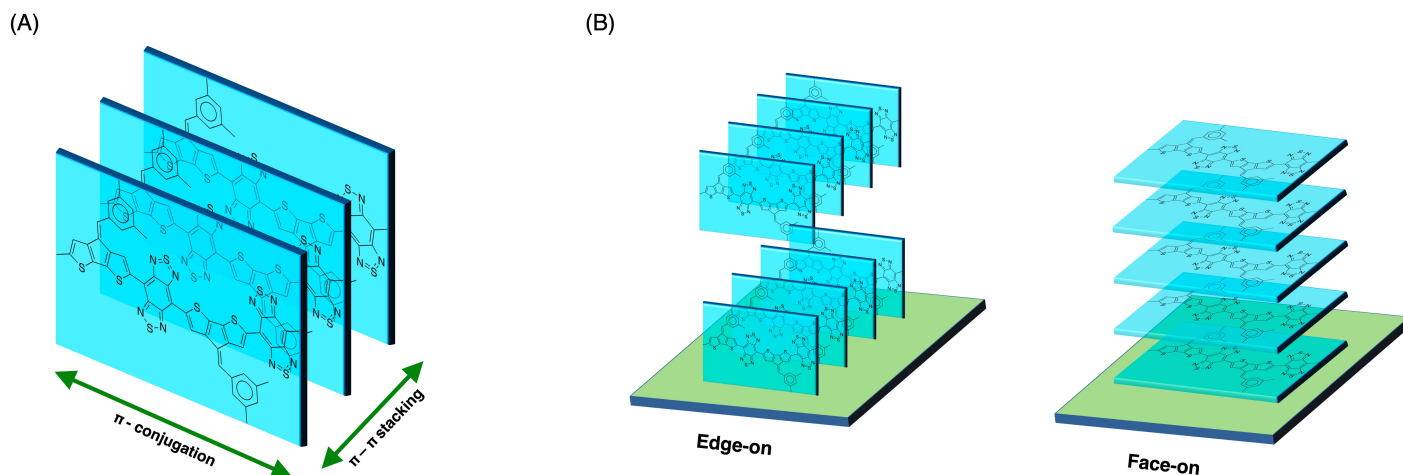


Fig. 1 A schematic illustrating different stacking orientations in thin films. (A) The π -conjugation direction and π - π stacking of conjugated polymers. (B) The π -stacking orientations of edge-on (left) and face-on (right) in the out-of-plane and in-plane directions, respectively.

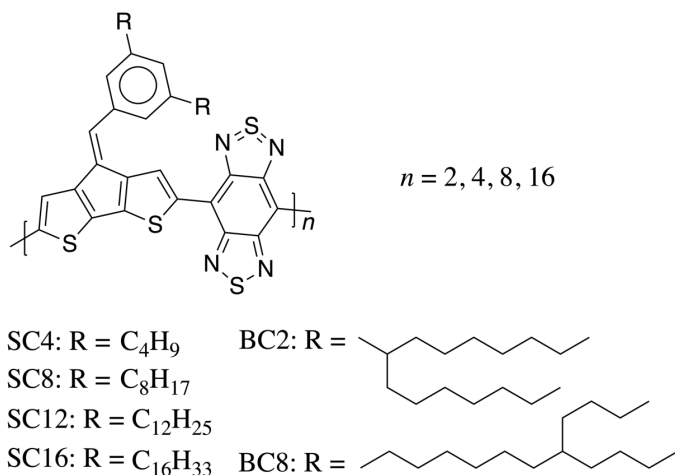


Fig. 2 Chemical structure of the CPDT-BBT polymer with the nomenclature for the linear side chains (SC) and branched side chains (BC).

ing the angle between aromatic ring planes as a function of the distance between ring centers, as seen in Fig. S3(E) and S3(F). The initial conformation of the oligomer chain was adopted from the optimized geometry obtained from the DFT calculations. This optimized structure represents a planar and extended conformation of the oligomer. The initial end-to-end distance of the oligomer chain is illustrated in Fig. 3, denoted as the length of an isolated single chain. The simulation box takes on a cubic shape, and periodic boundary conditions are applied to the system. The simulation box's length is approximately twice the correlation length, determined from the oligomers' radius of gyration (R_g) to minimize the system size effects. The correlation length (ξ) is closely related to the R_g of the polymers in a solution.⁵³ For dilute solutions, $R_g = \sqrt{3}\xi$, and in semi-dilute solutions, polymer chains tend to contract, causing R_g to become smaller.^{58,59} Therefore, the initial system box length is considered to be roughly twice the oligomer end-to-end distance, and during the production run, we ensure that the box length remains larger than twice the correlation length, as indicated in Table S2. As the chain

length of the oligomers increases from $n = 2$ to $n = 16$, the box lengths are adjusted accordingly, ranging from 11 to 40 nm. The initial configuration of the oligomer chains is based on the optimized geometry of CPDT-BBT obtained from quantum mechanical (QM) calculations. Typically, conjugated polymer thin films are prepared by spin-coating a dilute solution (~ 5 mg/ml) on a quartz substrate.^{7,10} During the spin coating, the solvent evaporates, and a thin polymer film is achieved. In our simulations, the concentration is approximately 50 mg/ml, representing an intermediate concentration between dilute solution and thin film. Thus, for each monomer of CPDT-BBT, we introduce 100 chloroform molecules to create the initial system. The system comprises 50 CPDT-BBT oligomers and the corresponding number of chloroform molecules. Notably, the chloroform force field (TraPPE) used in the simulation can reproduce the experimental density with a slight deviation (2.1% lower).^{60–62}

The initial system configuration was subjected to energy minimization (emtol = 1.0 [kJ mol⁻¹nm⁻¹]) lasting 1 ns, utilizing a time step of 1 fs. The system was further equilibrated through a constant volume and temperature (NVT, or canonical ensemble) simulation, spanning 25 ns with a time step of 2 fs. During this phase, the velocity-rescale⁶³ thermostat was employed to maintain the system at the desired temperature. Following the NVT simulation, a constant pressure and temperature (NPT, or isothermal-isobaric ensemble) simulation was conducted for an additional 25 ns, utilizing a time step of 2 fs. In the NPT ensemble, the pressure was set to 1 bar, regulated by the Berendsen barostat,⁶⁴ while the temperature was maintained via the velocity-rescale thermostat. Subsequently, the production run under the NPT ensemble conditions was carried out, spanning 700 ns with a time step of 2 fs. During this phase, the Nosé–Hoover thermostat^{65,66} and Parinello–Rahman barostat⁶⁷ were employed to control temperature and pressure, respectively. All molecular dynamics simulations were conducted using the Gromacs⁶⁸ package (version 2020.3). Short-range van der Waals and Coulombic interactions were truncated at a distance of 1.4 nm. Long-range Coulombic interactions were treated using particle-

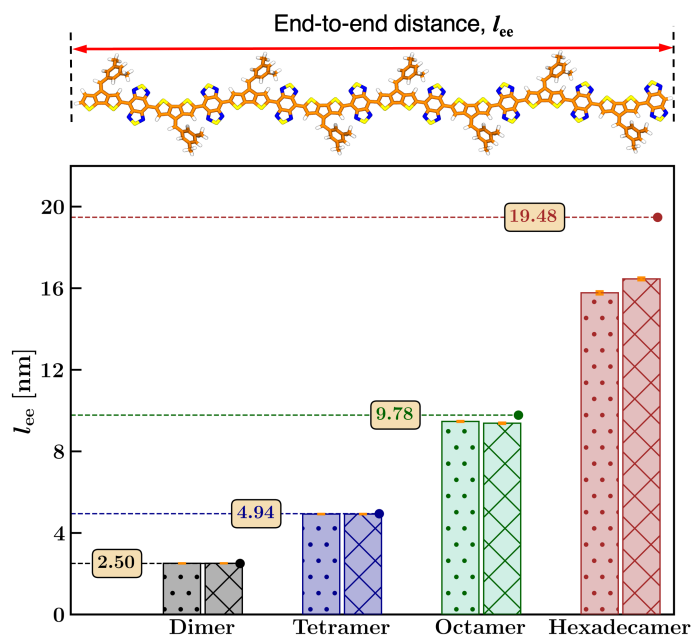


Fig. 3 The end-to-end distance of CPDT-BBT oligomers in the chloroform solvent as a function of chain length. The isolated single-chain elongated lengths are indicated by horizontal dashed lines and their respective values. Dotted bars represent data at $T = 298$ K, while crossed bars represent data at $T = 323$ K.

mesh Ewald (PME) summation, employing a cutoff distance of 1.4 nm and specific settings (PME order of 4 and Fourier spacing of 0.16 nm). Leapfrog time integration and LINCS bond constraints were applied to generate trajectories. All the properties are analyzed over the last 200 ns of trajectories unless explicitly stated in the Results and Discussion section.

3 Results and Discussion

3.1 Conformation Evolution

The end-to-end (*E2E*) distance, denoted as l_{ee} , serves as a structural parameter to understand the conformation flexibility (or the rigidity) of the polymer chains. It is the distance between the two termini of the oligomer chain. The extended conformation of the isolated CPDT-BBT oligomer chains serves as a useful reference. By contrasting the l_{ee} value with that of a fully extended chain length, we can discern the conformational flexibility behavior of the oligomers. Upon analyzing the *E2E* distance, it becomes apparent that the average l_{ee} and the spread of the l_{ee} distribution ($\rho(l_{ee})$) increase with the oligomer chain length, as evident in Fig. 3 and Fig. S4, respectively. Specifically, the shorter oligomers exhibit more extended structures, whereas longer ones display greater curvature along the chain backbone. The influence of temperature remains less pronounced for shorter oligomers (up to $n = 8$). However, the hexadecamer ($n = 16$) demonstrates a moderately extended structure at the higher temperature ($T = 323$ K). Accompanying this, the distribution $\rho(l_{ee})$ appears broader, leading to a decrease in the peak height at $T = 323$ K, a trend illustrated in Fig. S4.

We examine the backbone twist to better understand the deviation in the *E2E* compared to the isolated chain extended con-

figuration. Analyzing the distribution $\rho(\phi)$ of the dihedral angle for the bond connecting the donor-acceptor moieties (highlighted by the red-colored bonds in Fig. 4) reveals a prominent peak around $\phi = \pm 20^\circ$. This signifies that the backbone retains an almost planar configuration while maintaining the initial trans conformation (as illustrated in Fig. S2). Interestingly, with increasing temperature, the peak height of $\rho(\phi)$ experiences a slight increase, particularly at $\phi = 0^\circ$, except for the octamer, where distributions remain nearly identical. This phenomenon leads to a narrower distribution as the chains adopt a more planar arrangement. During the progression from $n = 2$ to 16, denoting the increase in oligomer chain length, the population of chains with a dihedral angle of zero degrees diminishes. At the same time, the distribution of end-to-end (*E2E*) distances becomes broader. The potential energy surface scan (refer to Fig. S1(H)) indicates that the dihedral minimum in energy is at approximately $\phi = 5^\circ$. This suggests that the oligomers exhibit increased twisting along the backbone due to intricate solvent and polymer and polymer-polymer interactions. The planar and elongated structure of CPDT-BBT plays a pivotal role in the stacking behavior of the oligomer chains, which will be discussed in detail in the subsequent section.

3.2 Aggregation in Solution

The planar and extended structure of CPDT-BBT is linked to the degree of aggregation of oligomer chains. The radial distribution function (RDF, $g(r)$) of the aromatic ring centers provides insights into this phenomenon, as depicted in Fig. 5. For shorter oligomers, a higher degree of ordered aggregation is evident. However, as the chain length increases, the packing and stacking become more disordered. Notably, the sections of oligomer chains that are $\pi - \pi$ stacked tend to be in closer proximity (indicated by the shift of the first RDF peak towards smaller distances). Furthermore, the chain ends of the backbones exhibit greater disorder and tend to stack with neighboring oligomers, facilitating the extension of aggregates along the polymer backbone. As can be seen in Fig. 6, the polymer ends (highlighted by pink circles) appear less ordered, while the stacked regions exhibit a more planar arrangement. Some oligomer chains act as bridges between distinct ordered aggregated regions, contributing to increased twisting of the oligomer backbones. Consistent

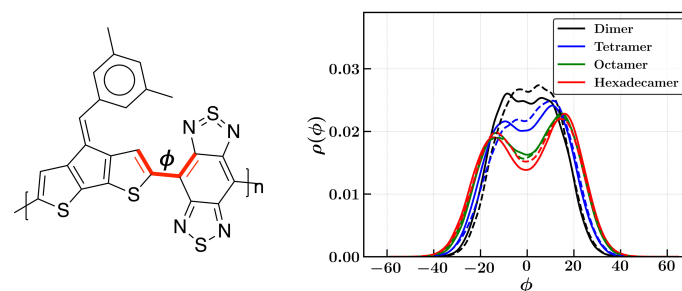


Fig. 4 The distribution ($\rho(\phi)$) of the torsion angle (ϕ) along the bond connecting the donor and acceptor, highlighted in red (left). The solid line corresponds to the distribution at $T = 298$ K, while the dashed line represents $T = 323$ K.

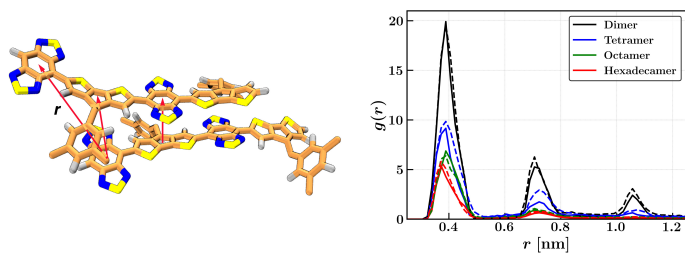


Fig. 5 Inter-chain RDFs ($g(r)$) for the aromatic ring-center along the CPDT-BBT backbone. The solid and dashed lines represent the distribution at $T = 298$ and 323 K, respectively.

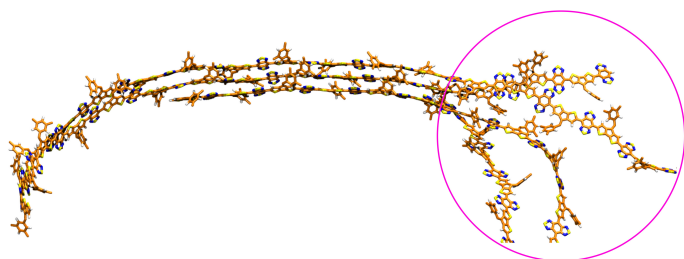


Fig. 6 Snapshot of polymer chain aggregate in chloroform for $n = 16$. A more significant chain disorder is observed near the chain ends (circled in pink).

with prior conformational analyses, the oligomers exhibit slightly enhanced stacking and ordered aggregation at the higher temperature.

To understand the dynamic evolution of CPDT-BBT aggregates in chloroform, we analyzed the cluster growth over the course of the simulation. Fig. 7 shows the number of clusters (N) and the size (specifically the largest cluster size, denoted as S) of the clusters over simulation time (t). The size of the largest cluster is defined as the number of oligomers (chains) within the largest cluster, with a maximum value of 50, given that each system contains 50 oligomers. A cutoff distance of 4 \AA , slightly larger than the first peak in the aromatic ring-center RDFs, is used to determine interchain connections within a cluster. In the initial stages of the simulation, longer oligomers ($n = 8$ and 16) quickly aggregate to form a large cluster. In contrast, slower cluster growth is observed for $n = 2$ and 4 as the simulation progresses. As cluster size increases, the total number of clusters decreases. Notably, cluster growth is more rapid at the higher temperature ($T = 323 \text{ K}$) due to the increased dynamics of the system, allowing oligomers to diffuse more rapidly.

Upon closer examination of CPDT-BBT aggregates, a distinct affinity for π - π stacking becomes evident. CPDT-BBT polymers exhibit a parallel displaced π - π stacking pattern with an average π -stacking distance (λ) of $3.38 \pm 0.03 \text{ \AA}$, similar to the experimentally determined value of 3.41 \AA .¹⁰ The average π -stacking distance shows variation with oligomer chain length, increasing from 3.34 \AA to 3.40 \AA as the chain length increases from dimer to octamer ($n = 2$ to 8), regardless of temperature ($T = 298 \text{ K}$ and 323 K), as depicted in Fig. 8. However, an intriguing exception is observed with the hexadecamer ($n = 16$), where the average π -stacking distance decreases to 3.35 \AA instead of increasing at

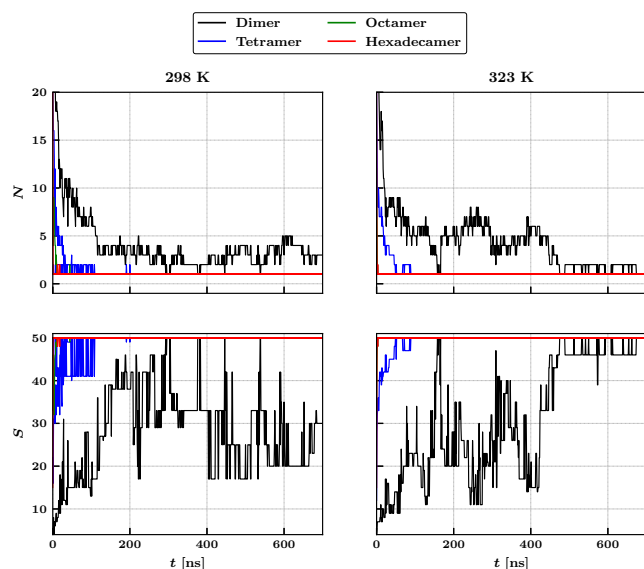


Fig. 7 The growth of clusters in terms of number of clusters (N) and size of the largest cluster (S), as a function of the oligomer size, are plotted as the simulation time (t). The left column for $T = 298 \text{ K}$ and the right column for $T = 323 \text{ K}$.

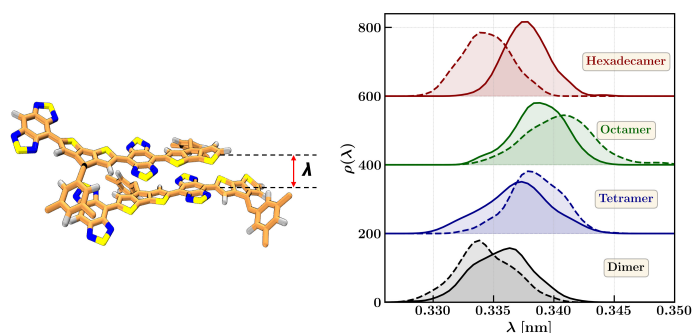


Fig. 8 The π - π stacking distribution of CPDT-BBT oligomers in chloroform. The solid and dashed lines represent the distribution at $T = 298$ and 323 K , respectively. A constant offset is applied on the y-axis to data for different oligomers.

both temperatures. At the lower temperature ($T = 298 \text{ K}$), the dimer and tetramer exhibit broader π -stacking distribution peaks, while the octamer and hexadecamer display sharper peaks (see Fig. S5). Interestingly, at the higher temperature ($T = 323 \text{ K}$), all oligomers, except the octamer, exhibit similar peak heights in their π -stacking distribution. This suggests that λ becomes more uniform with respect to oligomer length at the higher temperature compared to the lower temperature.

To better understand the molecular packing, we determine the displacement between neighboring CPDT-BBT oligomers, given their propensity for π - π stacking with parallel displacement. This displacement occurs in two primary directions: along the chain backbone or π -conjugation length (referred to as long displacement), and perpendicular to the chain backbone (referred to as short displacement), as illustrated in Fig. S6. At the lower temperature, the average long displacement (b_{long}) increases from 1.8 to 2.1 \AA as the oligomer chain length grows (shown in Table

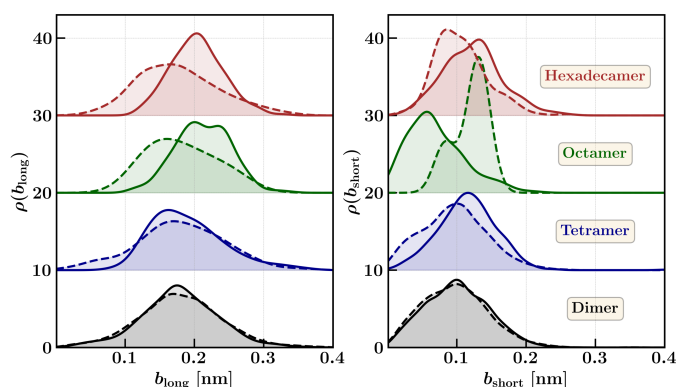


Fig. 9 The distribution of parallel displacement along the long-axis (left) and the short-axis (right). The solid and dashed lines represent the distribution at $T = 298$ K and 323 K, respectively. A constant offset is applied on the y-axis to data for different oligomers.

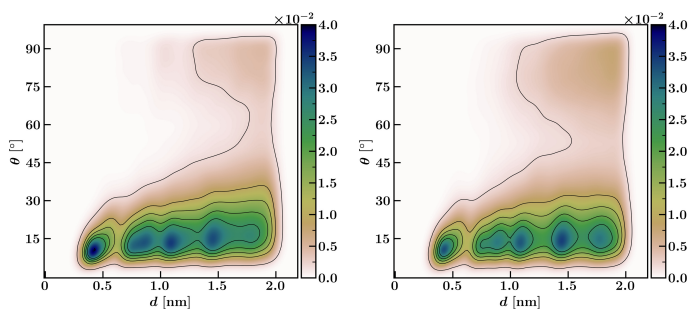


Fig. 10 The angle (θ) between the stacked aromatic rings (planes) is plotted as a function of the distance (d) between the ring centers. This result is for dimer ($n = 2$) at $T = 298$ K (left) and $T = 323$ K (right).

S3). They display a similar trend for displacement distance as we have observed for π - π stacking. The displacement distance increases from dimer to octamer, while for hexadecamer, it reduces. However, all the oligomers exhibit a consistent average b_{long} of approximately 1.8 \AA at the higher temperature. Furthermore, the distribution of short displacement ($\rho(b_{short})$) ranges between $1.0 - 1.2 \text{ \AA}$ for all the oligomers, except the octamer, as shown in Fig. 9, at both temperatures.

Fig. 10 illustrates the relationship between the angle formed by stacked aromatic rings (planes) and the distance separating the centers of these stacked rings. The density, represented as a heat map in Fig. 10, is highest at shorter distances (d) since the majority of oligomers stack with at least one neighboring oligomer. Conversely, there is a greater likelihood of finding stacked aromatic rings with an angle falling within the range of 5° to 15° . It suggests that the stacking between oligomers occurs with a near-parallel orientation. The angle (θ) between stacked ring centers increases with the distance (d) between them, a trend observed at both temperatures for all oligomers. Notably, there is a steep increase in angle with distance for longer oligomers, as depicted in Fig. S7. It can be attributed to the reduced order in stacked oligomers and diminished planarity observed between neighboring stacked chains in longer oligomers.

In the discussions thus far, we have only considered the regio-regular arrangement of the aromatic side group, where the side

groups are oriented towards the acceptor unit of the respective monomer. It naturally begs the question of how regio-regularity affects the aggregation behavior. To quantify the role of regio-regularity, we carried out additional simulations for the regio-irregular structure of tetramer where the aromatic side groups orientated towards and away from the acceptor moiety (see Fig. S8). Interestingly, the regio-regularity does not affect the end-to-end distance (Fig. S8). The average π - π stacking and displacement (both long and short) also show behavior similar to the regio-regular conformation, as depicted in Fig. S9 and S10, respectively. The distribution of the dihedral angle of the donor-acceptor adjoining angle in Fig. 11 (A) also suggests that regio-irregularity has negligible impact. The introduction of regio-irregularity, however, does lead to increased backbone twisting in a specific direction due to steric repulsion effects. This twisting is primarily caused by the lateral groups being oriented towards the same acceptor. In contrast, when the lateral groups point away from the nearby acceptor, they contribute to enhanced flexibility and help maintain a planar backbone structure, as indicated in Fig. 11 (B). These findings underscore the intricate interplay between lateral group orientation, steric effects, and overall molecular conformation of the polymer.

The solvent quality and interactions with solvent molecules influence the conformation of polymer chains in a solution. In the case of CPDT-BBT oligomers, chloroform (the solvent) molecules exhibit distinct interactions. Fig. 12 illustrates the radial distribution function (RDF), $g(r)$, of solvent molecules around the sulfur (S) and nitrogen (N) atoms of the polymer. Notably, the solvent density near the S atoms surpasses that near the N atoms of CPDT-BBT. This behavior is consistently observed, as demonstrated by the regio-irregular conformation of the CPDT-BBT tetramer in Fig. S11. The position of the lateral groups primarily affects solvent density near S-BBT, while the density near N-BBT remains relatively constant, regardless of the lateral group's orientation. Concurrently, the first solvation shell exhibits a higher peak for the

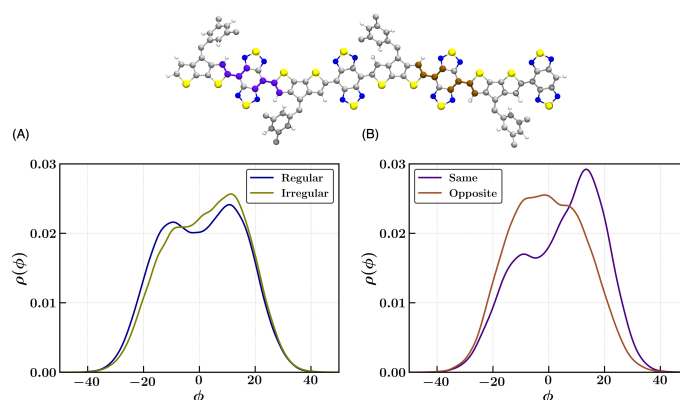


Fig. 11 The distribution ($\rho(\phi)$) represents the frequency of occurrence of the torsion angle (ϕ) along the bond that connects the donor and acceptor moieties. (A) The torsion angle distribution for both regio-regular and regio-irregular conformations of the CPDT-BBT tetramer is shown. (B) The distribution of the dihedral angle is shown when the lateral group points towards the same acceptor (purple) and when it points towards the opposite acceptor (brown). These dihedral angles are depicted on the top image of the CPDT-BBT tetramer.

S atoms of BBT (acceptor) moieties (S-BBT) compared to the S atoms of CPDT (donor) moieties (S-CPDT). This suggests a preference for solvent molecules to be in close proximity to S-BBT than S-CPDT, driven by distinct Coulomb interactions between the S atoms of donor and acceptor moieties. Notably, the first solvation shell peaks for S-CPDT and N-BBT are approximately 4.0 Å, whereas that for S-BBT extends to around 4.5 Å. At the higher temperature, indicated by the dashed lines in Fig. 12, the height of the first solvation peak undergoes a slight reduction, signifying a moderate decrease in solvent structure around the polymer chain at the higher temperature.

3.3 Effect of the Side Chain on the Aggregation Behavior

To observe the effect of the side chain on the aggregation behavior, we considered only the octamer system. From the E2E distance analysis, it is evident that the side chains help to increase the polymer chain distortion as the distribution of l_{ee} or $\rho(l_{ee})$ becomes broader and the height of the peak of $\rho(l_{ee})$ decreases as shown in Fig. S12. With the increase of side chain length from SC4 (C₄) to SC16 (C₁₆), the average E2E distance increases from 9.1 nm to 9.4 nm (see Fig. S12 (left)). But the height of the peak of $\rho(l_{ee})$ becomes smaller, which confirms that the longer alkyl side chains increase the backbone distortion. To examine the impact of branching position in alkyl side chains, a fixed length of the alkyl chain of C₁₆ is considered with a branching point at C₂ (BC2) or C₈ (BC8). The branching position effect on E2E distance is compared with the linear side chain of the length of C₁₆ (SC16) and with the octamer of CPDT-BBT (no side chain) as shown in Fig. S12 (right). It reveals that the CPDT-BBT with branched chains (BC) shows fewer distortions and lower average E2E distance than CPDT-BBT with linear chains (SC). CPDT-BBT exhibits

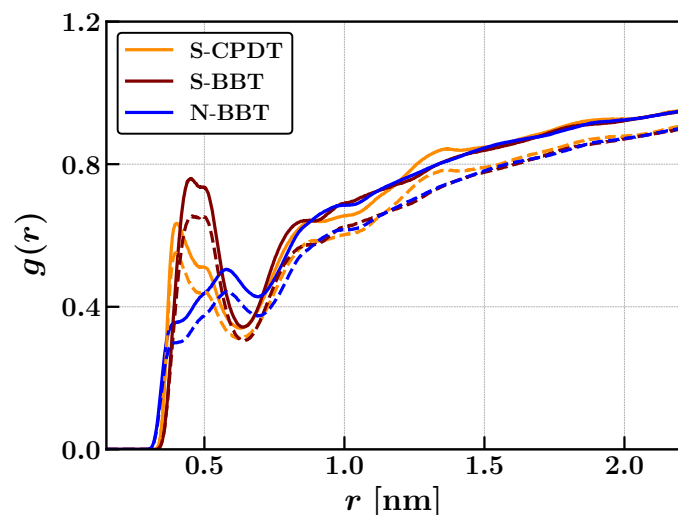


Fig. 12 Radial distribution function (RDF), $g(r)$, of solvent (chloroform) molecules around the CPDT-BBT oligomers. The RDF is plotted as a function of distance (r) between C-atoms (carbon) of chloroform and S-atoms in CPDT moieties (orange), C-atoms of chloroform and S-atoms in BBT moieties (maroon), and C-atoms of chloroform and N-atoms in BBT moieties (blue). The solid and dashed lines represent the distribution at $T = 298$ and 323 K, respectively.

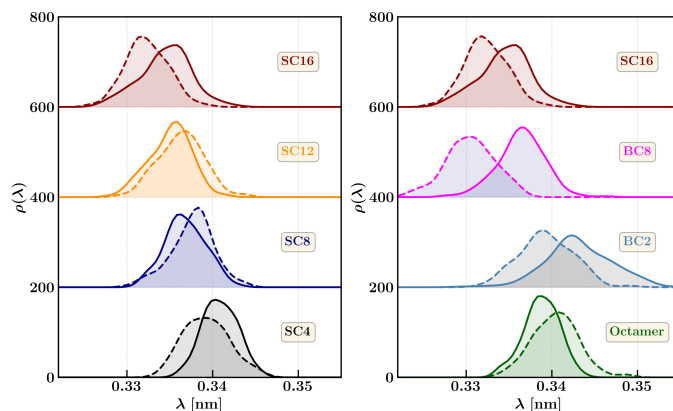


Fig. 13 The π - π stacking distribution of octamer with linear alkyl side chains (left) and branched alkyl side chains (right) in chloroform solvent. The linear side chain length varies as C₄ (SC4), C₈ (SC8), C₁₂ (SC12), C₁₆ (SC16) (left). The branching position (at C₂ (BC2) and C₈ (BC8)) effect is compared with the same length of linear side chain C₁₆ (SC16) and the octamer with no side chains (right). The solid and dashed lines represent the distribution at $T = 298$ and 323 K, respectively. A constant offset is applied on the y-axis to data for different side chains.

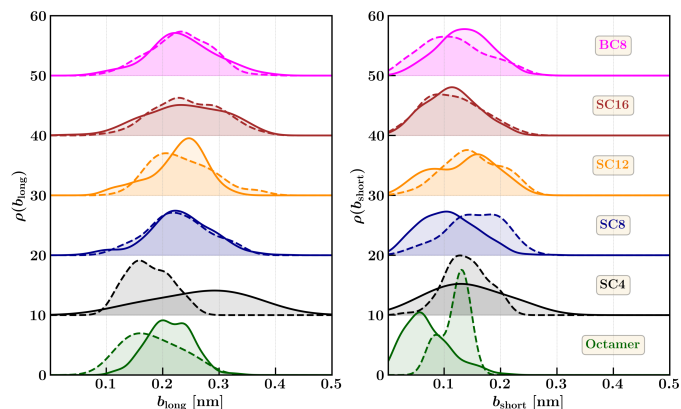


Fig. 14 The distribution of displacement along the long-axis (left) and short-axis (right) of CPDT-BBT with different alkyl side chains. Linear side chains are represented as SC, while the number represents the length of the alkyl chains. Branched side chains are represented as BC, while the number represents the branching positions. The solid and dashed lines represent the distribution at $T = 298$ K and 323 K, respectively. A constant offset is applied on the y-axis to data for different side chains.

a more extended structure as the branching position moves away from the backbone (BC2 to BC8). CPDT-BBT with different side chains displays a slightly more extended structure at the lower temperature, while their degree of distortion remains the same at both temperatures. The D-A dihedral distribution (Fig. S13) reveals no significant effect of linear alkyl side chains on CPDT-BBT backbone twisting, which is true for both temperatures. The CPDT-BBT with a closer branching point (BC2) exhibits slightly more twist than the farther (BC8) one.

The length and branching positions of alkyl side chains have a notable impact on the average π - π stacking distance (λ). As depicted in Fig. 13 (left), increasing the linear alkyl side chain length leads to a reduction in λ . This occurs because longer alkyl side chains promote better solvation of the oligomers and encour-

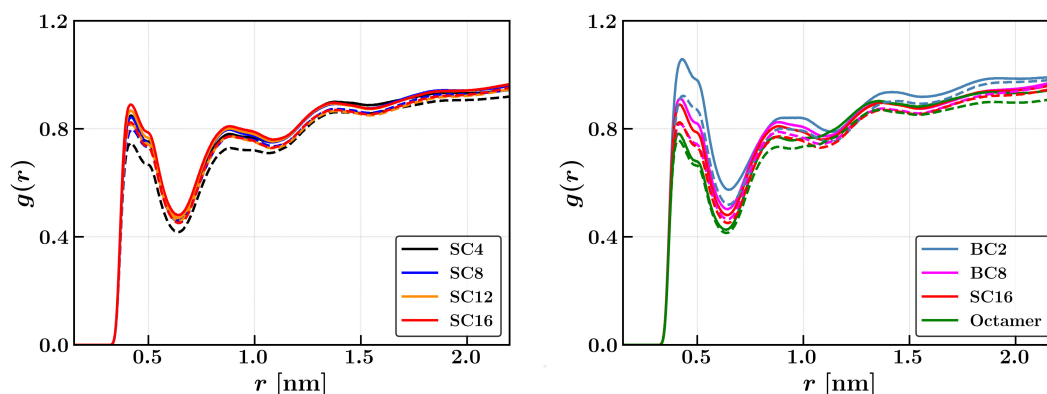


Fig. 15 The radial distribution function of solvent (chloroform) molecules around the CPDT-BBT oligomers. The RDF is plotted as a function of distance (r) between C-atoms (carbon) of chloroform and S-atoms in CPDT moieties. Linear side chains are represented as SC, while the number represents the length of the alkyl chains (left). Branched side chains are represented as BC, while the number represents the branching positions (right). The solid and dashed lines represent the distribution at $T = 298$ and 323 K, respectively.

age stronger face-to-face interactions, resulting in a smaller π -stacking distance. Furthermore, the position of branching on the side chains plays a role. Oligomers with a closer branching point (BC2) exhibit moderately higher λ compared to those with a farther branching point (BC8), primarily due to steric repulsion (as seen in Fig. 13, right). It's worth noting that oligomers with side chains (BC8 and SC16) have a smaller average π - π stacking distance (λ) than the octamer without side chains. This is because side chains enhance solvation in the chloroform solvent. Additionally, at the higher temperature, oligomers with side chains display a shorter average π - π stacking distance compared to the lower temperature.

At the elevated temperature ($T = 323$ K), the displacement along the long axis of CPDT-BBT increases from 1.8 \AA to 2.4 \AA as the alkyl side chains lengthen, as depicted in Fig. 14. Conversely, at the lower temperature ($T = 298$ K), the long-axis displacement ranges from 2.3 \AA to 2.7 \AA , showing variation with the side chain length. In contrast, the short-axis displacement exhibits a similar range for both temperatures, fluctuating between 1.1 \AA to 1.5 \AA as shown in Table S4. CPDT-BBT with the branching side chain BC2 does not exhibit complete stacking within the simulation time frame necessary to measure displacement. Furthermore, CPDT-BBT with side chains shows a reduced number of π - π stacking interactions, further decreasing with increasing alkyl side chain length, as shown in Fig. S14. This reduction in stacking interactions is attributed to steric hindrance. CPDT-BBT, with a closer branching position (BC2) near the backbone, exhibits fewer π - π stacking interactions with neighboring CPDT-BBT molecules. Oligomers with shorter side chains aggregate more rapidly and form long-range aggregates. Therefore, the increased flexibility observed in CPDT-BBT with longer side chains is due to the limited π - π stacking interactions among neighboring oligomers. Cluster formation occurs more rapidly at the higher temperature ($T = 323$ K) for CPDT-BBT in chloroform solvent, as depicted in Fig. S15. However, the presence of branched alkyl side chains results in a delay in cluster formation.

The solvent structure near CPDT-BBT increases slightly with the increasing alkyl side chain length, as depicted in Fig. 15 (left).

The alkyl side chains enhance the solvation of CPDT-BBT in chloroform solvent. Fig. 15 (right) reveals that CPDT-BBT with a closer (BC2) branched alkyl chain experiences better solvation in chloroform solvent than CPDT-BBT with a farther (BC8) branched chain. Moreover, the branching of alkyl side chains contributes to improved solvation of CPDT-BBT in chloroform solvent. Notably, CPDT-BBT exhibits superior solvation in chloroform solvent at a lower temperature ($T = 298$ K) compared to a higher temperature ($T = 323$ K).

4 Conclusions

Our extensive molecular dynamics simulations elucidate the aggregation behavior of high-spin organic conjugated polymers in chloroform. We investigated the effect of chain length, side chain, regioregularity, and temperature on polymer aggregation and conformation. Our findings indicate that CPDT-BBT oligomers strongly favor π - π stacking, a pivotal factor in their aggregation behavior. Chain length, side chain length, and branching positions influence the average π - π stacking distance, with shorter chains exhibiting more ordered aggregation. Side chain length and branching position significantly affect backbone twist, with longer linear side chains promoting smaller stacking distances. When the branching point in the side chain is closer to the polymer backbone, it results in slightly higher stacking distances due to steric effects, emphasizing the importance of side chain design. Regioregularity mainly impacts the backbone twisting rather than the overall assembly. Regio-irregularity induces steric repulsion, increasing twisting, while groups facing away from nearby acceptors promote planarity. Temperature influences aggregation behavior, with the higher temperature leading to faster aggregation kinetics. However, over the small temperature range considered here, temperature has only a very minor impact on the organization and structure of aggregates. Solvent density distribution reveals a preference for sulfur (S) atoms over nitrogen (N) atoms in CPDT-BBT, consistent across regio-irregular conformations. Our study underscores the interplay of polymer structure, solvent interactions, and environmental factors control aggregation of conjugated polymers in the liquid phase.

Conflicts of interest

There are no conflicts to declare.

Acknowledgements

This work is supported by National Science Foundation (NSF) under the award OIA-1757220. This research used computational resources at the High Performance Computing Collaboratory at Mississippi State University. We acknowledge the Texas Advanced Computing Center (TACC) at the University of Texas at Austin for providing HPC, Stampede 2 (through the Extreme Science and Engineering Discovery Environment (XSEDE)⁶⁹ supported by NSF grant number ACI-1548562) allocation (TG-CHE140141) for computational resources.

References

- 1 A. Rajca, J. Wongsriratanakul and S. Rajca, *Science*, 2001, **294**, 1503–1505.
- 2 N. M. Gallagher, A. Olankitwanit and A. Rajca, *J. Org. Chem.*, 2015, **80**, 1291–1298.
- 3 M. A. Sabuj, O. Muoh, M. M. Huda and N. Rai, *Phys. Chem. Chem. Phys.*, 2022, **24**, 23699–23711.
- 4 S. Sanvito, *Chem. Soc. Rev.*, 2011, **40**, 3336–3355.
- 5 M. A. Sabuj, C. Saha, M. M. Huda and N. Rai, *Mol. Syst. Des. Eng.*, 2023.
- 6 M. Abe, *Chem. Rev.*, 2013, **113**, 7011–7088.
- 7 A. E. London, H. Chen, M. A. Sabuj, J. Tropp, M. Saghayezhian, N. Eedugurala, B. Zhang, Y. Liu, X. Gu, B. Wong, N. Rai and J. Azoulay, *Sci. Adv.*, 2019, **5**, eaav2336.
- 8 M. A. Sabuj, M. M. Huda, C. S. Sarap and N. Rai, *Mater. Adv.*, 2021, **2**, 2943–2955.
- 9 K. Wang, L. Huang, N. Eedugurala, S. Zhang, M. A. Sabuj, N. Rai, X. Gu, J. D. Azoulay and T. N. Ng, *Adv. Energy Mater.*, 2019, **9**, 1902806.
- 10 M. E. Steelman, D. J. Adams, K. S. Mayer, P. Mahalingavelar, C.-T. Liu, N. Eedugurala, M. Lockart, Y. Wang, X. Gu and M. K. Bowman, *Adv. Mater.*, 2022, **34**, 2206161.
- 11 T. L. D. Tam, G. Wu, S. W. Chien, S. F. V. Lim, S.-W. Yang and J. Xu, *ACS Mater. Lett.*, 2020, **2**, 147–152.
- 12 T. Marszalek, M. Li and W. Pisula, *Chem. Commun.*, 2016, **52**, 10938–10947.
- 13 H. Ahmad, S. Zhang, C.-T. Liu, G. Ma, J. D. Azoulay, X. Gu, M. K. Gangishetty and S. Kundu, *ACS Appl. Polym. Mater.*, 2022.
- 14 Z. Xiao, K. Sun, J. Subbiah, T. Qin, S. Lu, B. Purushothaman, D. J. Jones, A. B. Holmes and W. W. Wong, *Polym. Chem.*, 2015, **6**, 2312–2318.
- 15 C. Liu, K. Wang, X. Hu, Y. Yang, C.-H. Hsu, W. Zhang, S. Xiao, X. Gong and Y. Cao, *ACS Appl. Mater. Interfaces*, 2013, **5**, 12163–12167.
- 16 H. Zhou, L. Yang, S. Xiao, S. Liu and W. You, *Macromolecules*, 2010, **43**, 811–820.
- 17 S.-F. Yang, Z.-T. Liu, Z.-X. Cai, M. J. Dyson, N. Stingelin, W. Chen, H.-J. Ju, G.-X. Zhang and D.-Q. Zhang, *Adv. Sci.*, 2017, **4**, 1700048.
- 18 S. B. Darling and M. Sternberg, *J. Phys. Chem. B*, 2009, **113**, 6215–6218.
- 19 J. S. Lee, S. K. Son, S. Song, H. Kim, D. R. Lee, K. Kim, M. J. Ko, D. H. Choi, B. Kim and J. H. Cho, *Chem. Mater.*, 2012, **24**, 1316–1323.
- 20 B. McCulloch, V. Ho, M. Hoarfrost, C. Stanley, C. Do, W. T. Heller and R. A. Segalman, *Macromolecules*, 2013, **46**, 1899–1907.
- 21 F. L. Lee, A. Barati Farimani, K. L. Gu, H. Yan, M. F. Toney, Z. Bao and V. S. Pande, *J. Phys. Chem. Lett.*, 2017, **8**, 5479–5486.
- 22 T. J. Fauvell, T. Zheng, N. E. Jackson, M. A. Ratner, L. Yu and L. X. Chen, *Chem. Mater.*, 2016, **28**, 2814–2822.
- 23 S. E. Root, N. E. Jackson, S. Savagatrup, G. Arya and D. J. Lipomi, *Energy Environ. Sci.*, 2017, **10**, 558–569.
- 24 P. J. Flory, *Principles of polymer chemistry*, Cornell University Press, 1953.
- 25 T.-Q. Nguyen, I. B. Martini, J. Liu and B. J. Schwartz, *J. Phys. Chem. B*, 2000, **104**, 237–255.
- 26 P. Cheng, C. Yan, Y. Li, W. Ma and X. Zhan, *Energy Environ. Sci.*, 2015, **8**, 2357–2364.
- 27 M. Brinkmann, L. Hartmann, L. Biniek, K. Tremel and N. Kayunkid, *Macromol. Rapid Commun.*, 2014, **35**, 9–26.
- 28 T. Li, H. Zhang, B. Liu, T. Ma, J. Lin, L. Xie and D. Lu, *Macromolecules*, 2020, **53**, 4264–4273.
- 29 S. R. Chaudhari, J. M. Griffin, K. Broch, A. Lesage, V. Lemaury, D. Dudenko, Y. Olivier, H. Sirringhaus, L. Emsley and C. P. Grey, *Chem. Sci.*, 2017, **8**, 3126–3136.
- 30 H. Zhang, T. Li, T. Ma, B. Liu, J. Ren, J. Lin, M. Yu, L. Xie and D. Lu, *J. Phys. Chem. C*, 2019, **123**, 27317–27326.
- 31 C. P. Callaway, A. L. Liu, R. Venkatesh, Y. Zheng, M. Lee, J. C. Meredith, M. Grover, C. Risko and E. Reichmanis, *ACS Appl. Mater. Interfaces*, 2022, **14**, 3613–3620.
- 32 J. K. Keum, K. Xiao, I. N. Ivanov, K. Hong, J. F. Browning, G. S. Smith, M. Shao, K. C. Littrell, A. J. Rondinone and E. A. Payzant, *CrystEngComm*, 2013, **15**, 1114–1124.
- 33 O. Wodo and B. Ganapathysubramanian, *Comput. Mater. Sci.*, 2012, **55**, 113–126.
- 34 O. Wodo and B. Ganapathysubramanian, *Appl. Phys. Lett.*, 2014, **105**, 153104.
- 35 G. M. Whitesides and M. Boncheva, *Proc. Natl. Acad. Sci.*, 2002, **99**, 4769–4774.
- 36 C. Sutton, C. Risko and J.-L. Bredas, *Chem. Mater.*, 2016, **28**, 3–16.
- 37 H. Sirringhaus, P. Brown, R. Friend, M. M. Nielsen, K. Bechgaard, B. Langeveld-Voss, A. Spiering, R. A. Janssen, E. Meijer and P. Herwig, *Nature*, 1999, **401**, 685–688.
- 38 D. T. Duong, M. F. Toney and A. Salleo, *Phys. Rev. B*, 2012, **86**, 205205.
- 39 M. Yoneya, S. Matsuoaka, J. Tsutsumi and T. Hasegawa, *J. Mater. Chem. C*, 2017, **5**, 9602–9610.
- 40 R. Kroon, D. A. Mengistie, D. Kiefer, J. Hynynen, J. D. Ryan, L. Yu and C. Müller, *Chem. Soc. Rev.*, 2016, **45**, 6147–6164.
- 41 D. Wang, Y. Yuan, Y. Mardiyati, C. Bubeck and K. Koynov,

- Macromolecules*, 2013, **46**, 6217–6224.
- 42 M. G. Martin and J. I. Siepmann, *J. Phys. Chem. B*, 1998, **102**, 2569–2577.
- 43 C. D. Wick, M. G. Martin and J. I. Siepmann, *J. Phys. Chem. B*, 2000, **104**, 8008–8016.
- 44 N. Lubna, G. Kamath, J. J. Potoff, N. Rai and J. I. Siepmann, *J. Phys. Chem. B*, 2005, **109**, 24100–24107.
- 45 N. Rai and J. I. Siepmann, *J. Phys. Chem. B*, 2007, **111**, 10790–10799.
- 46 N. Rai and J. I. Siepmann, *J. Phys. Chem. B*, 2013, **117**, 273–288.
- 47 W. L. Jorgensen and J. Tirado-Rives, *Proc. Natl. Acad. Sci.*, 2005, **102**, 6665–6670.
- 48 J.-D. Chai and M. Head-Gordon, *Phys. Chem. Chem. Phys.*, 2008, **10**, 6615–6620.
- 49 T. Körzdörfer and J.-L. Brédas, *Acc. Chem. Res.*, 2014, **47**, 3284–3291.
- 50 A. Karpfen, C. H. Choi and M. Kertesz, *J. Phys. Chem. A*, 1997, **101**, 7426–7433.
- 51 C. Sutton, T. Körzdörfer, M. T. Gray, M. Brunfeld, R. M. Parrish, C. D. Sherrill, J. S. Sears and J.-L. Brédas, *J. Chem. Phys.*, 2014, **140**, 054310.
- 52 L. Kronik, T. Stein, S. Refaely-Abramson and R. Baer, *J. Chem. Theory Comput.*, 2012, **8**, 1515–1531.
- 53 K. Do, M. K. Ravva, T. Wang and J.-L. Brédas, *Chem. Mater.*, 2017, **29**, 346–354.
- 54 M. J. Frisch, G. W. Trucks, H. B. Schlegel, G. E. Scuseria, M. A. Robb, J. R. Cheeseman, G. Scalmani, V. Barone, G. A. Petersson, H. Nakatsuji, X. Li, M. Caricato, A. V. Marenich, J. Bloino, B. G. Janesko, R. Gomperts, B. Mennucci, H. P. Hratchian, J. V. Ortiz, A. F. Izmaylov, J. L. Sonnenberg, D. Williams-Young, F. Ding, F. Lipparini, F. Egidi, J. Goings, B. Peng, A. Petrone, T. Henderson, D. Ranasinghe, V. G. Zakrzewski, J. Gao, N. Rega, G. Zheng, W. Liang, M. Hada, M. Ehara, K. Toyota, R. Fukuda, J. Hasegawa, M. Ishida, T. Nakajima, Y. Honda, O. Kitao, H. Nakai, T. Vreven, K. Throssell, J. A. Montgomery, Jr., J. E. Peralta, F. Ogliaro, M. J. Bearpark, J. J. Heyd, E. N. Brothers, K. N. Kudin, V. N. Staroverov, T. A. Keith, R. Kobayashi, J. Normand, K. Raghavachari, A. P. Rendell, J. C. Burant, S. S. Iyengar, J. Tomasi, M. Cossi, J. M. Millam, M. Klene, C. Adamo, R. Cammi, J. W. Ochterski, R. L. Martin, K. Morokuma, O. Farkas, J. B. Foresman and D. J. Fox, *Gaussian16 Revision C.01*, 2016, Gaussian Inc. Wallingford CT.
- 55 L. S. Dodda, I. Cabeza de Vaca, J. Tirado-Rives and W. L. Jorgensen, *Nucleic Acids Res.*, 2017, **45**, W331–W336.
- 56 A. V. Marenich, S. V. Jerome, C. J. Cramer and D. G. Truhlar, *J. Chem. Theory Comput.*, 2012, **8**, 527–541.
- 57 L. Martínez, R. Andrade, E. G. Birgin and J. M. Martínez, *J. Comput. Chem.*, 2009, **30**, 2157–2164.
- 58 B. Hammouda and D. L. Ho, *J. Polym. Sc. B: Polym. Phys.*, 2007, **45**, 2196–2200.
- 59 I. Teraoka, *Polymer solutions*, 2002.
- 60 G. Kamath, G. Georgiev and J. J. Potoff, *J. Phys. Chem. B*, 2005, **109**, 19463–19473.
- 61 A. Mulero and M. Parra, *Phys. Chem. Liq.*, 2008, **46**, 263–277.
- 62 R. A. Clará, A. C. Gómez Marigliano, D. Morales and H. N. Sólamo, *J. Chem. Eng. Data*, 2010, **55**, 5862–5867.
- 63 G. Bussi, D. Donadio and M. Parrinello, *J. Chem. Phys.*, 2007, **126**, 014101.
- 64 H. J. Berendsen, J. v. Postma, W. F. van Gunsteren, A. DiNola and J. R. Haak, *J. Chem. Phys.*, 1984, **81**, 3684–3690.
- 65 S. Nosé, *Mol. Phys.*, 1984, **52**, 255–268.
- 66 W. G. Hoover, *Phys. Rev. A*, 1985, **31**, 1695.
- 67 M. Parrinello and A. Rahman, *J. Appl. Phys.*, 1981, **52**, 7182–7190.
- 68 M. J. Abraham, T. Murtola, R. Schulz, S. Páll, J. C. Smith, B. Hess and E. Lindahl, *SoftwareX*, 2015, **1**, 19–25.
- 69 J. Towns, T. Cockerill, M. Dahan, I. Foster, K. Gauthier, A. Grimshaw, V. Hazlewood, S. Lathrop, D. Lifka and G. D. Peterson, *Comput. Sc. Eng.*, 2014, **16**, 62–74.